RSC Pharmaceutics

ROYAL SOCIETY OF CHEMISTRY

PAPER

View Article Online
View Journal | View Issue

Cite this: *RSC Pharm.*, 2025, **2**, 1458

Redefining LNP composition: phospholipid and sterol-driven modulation of mRNA expression and immune outcomes

Muattaz Hussain,[a] Ashish Muglikar,[a] Danielle E. Brain,[b,c] Alexander J. Plant-Hately,[b,c] Neill J. Liptrott,[b,c] Daragh M. McLoughlin[d] and Yvonne Perrie *[a]

Ionisable lipids are essential components of lipid nanoparticles (LNPs), enabling nucleic acid encapsulation, cellular uptake, and endosomal escape. Helper lipids further modulate LNP stability, biodistribution, and intracellular trafficking. This study evaluated the *in vitro* and *in vivo* performance of LNPs incorporating different phospholipids (DSPC, DOPC, DOPE) and sterols (cholesterol, β-sitosterol), using HEK293 cells and murine models. LNPs were prepared *via* microfluidics at a fixed molar ratio (phospholipid : sterol/DOPE : SM-102 : PEG-lipid, 10 : 38.5 : 50 : 1.5 mol%). All formulations demonstrated comparable critical quality attributes, including particle size (80–120 nm), low polydispersity index (<0.2), near-neutral zeta potential, and high mRNA encapsulation efficiency (>95%). LNPs containing β-sitosterol exhibited significantly enhanced luciferase protein expression *in vitro* compared to the cholesterol-based control LNPs. *In vivo*, DSPC/cholesterol LNPs achieved the highest intramuscular luciferase expression, whereas DOPE-containing LNPs showed low expression. Immunisation studies showed that DOPE-containing LNPs generally enhanced total IgG and IgG1 responses, whereas IgG2a titres varied, with DOPC/DOPE highest and DSPC/DOPE lowest, indicating a disconnect between protein expression and immunogenicity. *Ex vivo* human whole blood assays revealed distinct cytokine profiles depending on sterol content. β-Sitosterol-incorporated LNPs induced elevated levels of TNF-α, GM-CSF, IL-8, IL-1β, IL-1RA, and IL-6, reflecting both pro- and anti-inflammatory activity, potentially *via* inflammasome activation. These findings demonstrate that phospholipid and sterol identity substantially influence both delivery efficiency and the quality of immune responses, emphasising the need to optimise the full lipid composition to tailor LNP performance for specific therapeutic applications.

Received 30th May 2025,
Accepted 23rd August 2025

DOI: 10.1039/d5pm00150a

rsc.li/RSCPharma

Introduction

Messenger RNA (mRNA) therapeutics have emerged as a transformative modality in modern medicine, enabling rapid-response vaccines, transient protein expression, and potential applications in gene editing and immuno-oncology. However, the inherent instability of mRNA and its susceptibility to rapid degradation by nucleases present substantial challenges for delivery. To address these limitations, lipid nanoparticles (LNPs) have become the leading non-viral delivery platform, capable of encapsulating, protecting, and efficiently delivering mRNA to target cells.

LNPs typically comprise four key lipid components: an ionisable lipid, a structural phospholipid, cholesterol, and a polyethylene glycol (PEG)-lipid conjugate. The ionisable lipid condenses the mRNA through electrostatic interactions during formulation and facilitates endosomal escape after cellular uptake. These lipids are designed to be positively charged at low pH (with $pK_a \sim 6.0$–6.5), but remain neutral at physiological pH, thereby reducing systemic toxicity and improving biocompatibility.[1] The structural phospholipid, often 1,2-distearoyl-*sn-glycero*-3-phosphocholine (DSPC), contributes to bilayer stability and particle integrity by forming tightly packed lamellar structures.[1] Cholesterol, a key membrane modulator, intercalates between phospholipid acyl chains to influence membrane fluidity, rigidity, and phase behaviour, enhancing LNP stability. The PEG-lipid (*e.g.* DMG-PEG2000) provides steric stabilisation and reduces aggregation.[1–3]

Although significant effort has been directed at optimising the ionisable lipid component, increasing attention is now

[a]*Strathclyde Institute of Pharmacy and Biomedical Sciences, University of Strathclyde, 161 Cathedral Street, G4 0RE Glasgow, UK.*
E-mail: Yvonne.perrie@strath.ac.uk
[b]*Immunocompatibility Group, University of Liverpool, Liverpool L7 8TX, UK*
[c]*Centre of Excellence for Long-Acting Therapeutics (CELT), University of Liverpool, Liverpool L7 8TX, UK*
[d]*Centre for Process Innovation (CPI), Coxon Building, John Walker Rd., Sedgefield, Stockton-on-Tees, TS21 3FE, UK*

being paid to the roles of the helper lipids, particularly the phospholipid and sterol components, in modulating the efficacy of LNPs. Structural lipids such as DSPC, 1,2-dioleoyl-*sn-glycero*-3-phosphocholine (DOPC), and 1,2-dioleoyl-*sn-glycero*-3-phosphoethanolamine (DOPE) differ in saturation and headgroup chemistry, which collectively affect their phase behaviour and interactions with endosomal membranes.[4] DOPE, for example, forms hexagonal phase structures under physiological conditions, promoting membrane fusion and enhancing endosomal escape.[5] In contrast, DSPC exhibits high rigidity and a high phase transition temperature, contributing to particle stability but potentially limiting membrane fusion and cellular uptake.[6]

Cholesterol plays a central but multifaceted role in LNP formulations. Its planar steroid ring structure enables it to insert between phospholipid tails, filling gaps and reducing permeability. This intercalation increases lipid packing density, modulates phase transitions, and enhances mechanical stability. While cholesterol is essential for maintaining LNP structure and colloidal stability, its direct involvement in endosomal escape mechanisms, such as membrane fusion and lipid mixing, remains less clearly defined. Some studies suggest that cholesterol may influence LNP membrane fluidity and curvature in ways that indirectly affect intracellular trafficking and endosomal release;[7] however, the precise mechanisms underlying cytosolic delivery remain poorly understood and require further investigation.[8]

Emerging evidence suggests that structural analogues of cholesterol can provide additional or improved functionality. For example, β-sitosterol, which differs from cholesterol by an ethyl group on its side chain, has been shown to enhance LNP-mediated transfection efficiency by modulating lipid packing and promoting membrane destabilisation.[7] Other analogues, such as oxidised sterols, may facilitate more efficient lipid mixing or promote negative membrane curvature that supports endosomal membrane rupture. These derivatives may destabilise the endosomal membrane by reducing its mechanical strength, thereby increasing permeability and promoting mRNA release.[7] Nonetheless, the precise mechanisms and optimal conditions for such enhancements remain to be fully elucidated.

Despite these findings, LNP formulations used in clinical settings still rely heavily on conventional combinations, such as those found in Spikevax, which contains DSPC, cholesterol, SM-102, and DMG-PEG2000 in a 10 : 38.5 : 50 : 1.5 molar ratio. While these combinations are effective, there is value in revisiting and potentially re-optimising LNP compositions for diverse delivery contexts, including different administration routes, target tissues, and therapeutic applications.

This study examines the impact of structural lipids and cholesterol identity on the physicochemical properties and biological performance of mRNA-loaded LNPs. Using a clinically validated LNP composition as a reference, we compare five formulations containing different combinations of DSPC, DOPC, DOPE, or β-sitosterol (Fig. 1). These formulations were evaluated based on their physicochemical characteristics, *in vitro* transfection efficiency, and *in vivo* expression and immunogenicity. By systematically varying these lipid components, we aim to elucidate their functional contributions and support the rational design of LNPs.

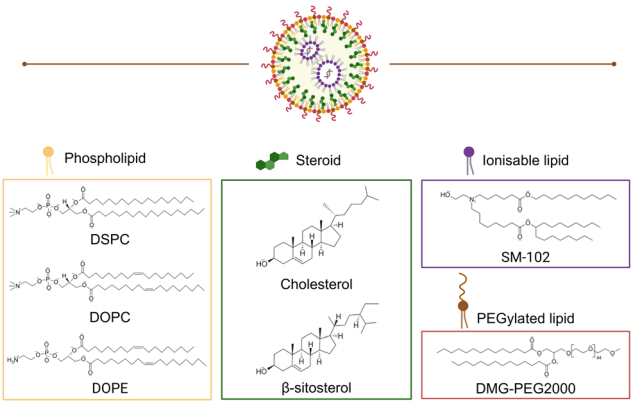

Fig. 1 Composition and key structural components of the lipid nanoparticles (LNPs) used in this study. The LNP formulations comprised four classes of lipids: (1) phospholipids: DSPC, DOPC, or DOPE (left, orange box); (2) sterols—cholesterol or β-sitosterol (centre, green box); (3) an ionisable lipid—SM-102 (top right, purple box); and (4) a PEGylated lipid—DMG-PEG2000 (bottom right, red box). Each lipid plays a distinct role in the formation, stability, and function of LNPs. The central illustration shows an LNP structure encapsulating mRNA (purple) within a lipid bilayer (multicoloured) assembled from the components tested.

Materials and methods

Materials

The ionisable lipid heptadecan-9-yl 8-{(2-hydroxyethyl)[6-oxo-6-(undecyloxy)hexyl]amino}octanoate (SM-102) was purchased from Broadpharm (San Diego, CA, USA). 1,2-Dioleoyl-*sn-glycero*-3-phosphoethanolamine (DOPE), 1,2-dioleoyl-*sn-glycero*-3-phosphocholine (DOPC), and 1,2-dimyristoyl-*rac-glycero*-3-methoxypolyethylene glycol-2000 (DMG-PEG2000) were purchased from Avanti Polar Lipids (Alabaster, AL, USA). 1,2-Distearoyl-*sn-glycero*-3-phosphocholine (DSPC) was obtained from Lipoid (Ludwigshafen, Germany). Cholesterol (Chol), β-sitosterol, citric acid, sodium citrate tribasic dehydrate, and polyadenylic acid (PolyA) were acquired from Merck Life Science (Hertfordshire, UK). Phosphate-buffered saline tablets (PBS pH 7.4) were acquired from Oxoid Ltd (Basingstoke, UK). Tris (hydroxymethyl) aminomethane (TRIS-base), DilC18(7) and ethanol (EtOH) were obtained from Fisher Scientific (Loughborough, UK). One-Glo luciferase Assay system and D-Luciferin + K (VivoGlo Luciferin) were purchased from Promega Ltd (Chilworth, UK). Messenger RNA (EZ Cap Firefly Luciferase mRNA, R1018-APE) was obtained from Stratech Scientific (Cambridgeshire, UK). Messenger RNA (Cap1 OVA mRNA) was obtained from OZ Biosciences SAS (Marseille, France). Minimal Essential Medium (MEM), fetal bovine serum (FBS), sodium pyruvate, and penicillin/streptomycin were acquired from Gibco Technologies. All solvents

and other chemicals were of analytical grade, and milliQ-water was provided by an in-house system.

Formulation of lipid nanoparticles (LNPs)

Lipid nanoparticles were formulated using the NanoAssemblr™ Ignite™ system (Cytiva, Vancouver, BC, Canada). The solvent phase consisted of lipids in ethanol at a molar ratio of 10 : 38.5 : 50 : 1.5 for DSPC or DOPC, cholesterol, DOPE or β-sitosterol, SM-102, and DMG-PEG2000, respectively (Table 1). The aqueous phase consisted of 50 mM citrate buffer (pH 4.0) containing either firefly luciferase (Fluc) mRNA or ovalbumin (OVA) mRNA at an N/P ratio of 6. The flow rate ratio (aqueous to organic) was set to 3 : 1, with a flow rate of 12 mL min^{-1}. DilC dyes were incorporated at a 1% molar ratio of the total lipid content to generate DilC-labelled PolyA LNPs for *in vitro* cellular uptake studies.

Removal of ethanol content and buffer exchange

LNP purification was performed using 100 kDa Amicon® Ultra centrifugal filter units (Merck Millipore Ltd, Hertfordshire, UK) by diluting the LNP formulations 1 : 40 in phosphate-buffered saline (PBS, pH 7.4), followed by centrifugation at 2000*g* and 20 °C until the desired LNP volume/concentration was recovered.

LNP characterisation: particle size, polydispersity and zeta potential

The particle size (*Z*-average diameter), polydispersity index (PDI), and zeta potential (ZP) of the LNPs were analysed using dynamic light scattering (DLS) with a Zetasizer Ultra (Malvern Panalytical Ltd, Worcestershire, UK). The system operated with a 633 nm laser and a detection angle of 173°. LNP samples were diluted in 0.22 μm-filtered PBS to a final lipid concentration of 0.1 mg mL^{-1}. A 4 mL cuvette was filled with 1000 μL of the diluted sample, using the same dilution for zeta potential measurements. The dispersant (PBS) had a refractive index (RI) of 1.330 and a viscosity of 0.8882 cP, while the material's absorbance and RI were 0.01 and 1.49, respectively. Zetasizer Software v.7.11 (Malvern Panalytical Ltd, Worcestershire, UK) was used for data acquisition. Each measurement was performed in triplicate, maintaining an attenuation value between 7 and 8.

Table 1 Composition of LNPs investigated in this study. The table outlines the lipid composition (percentage by molar ratio) of the LNP formulation, including the phospholipid (DSPC or DOPC), the steroid (cholesterol or β-sitosterol) or DOPE, the ionisable lipid (SM-102) and the PEG-lipid (DMG-PEG2000)

Formulation	10%	38.5%	50%	1.5%
1	DPSC	Chol	SM-102	DMG-PEG
2	DOPC	Chol		
3	DSPC	DOPE		
4	DOPC	DOPE		
5	DSPC	β-Sitosterol		

Quantification of PolyA and mRNA Loading

The encapsulation efficiency of PolyA/Fluc mRNA was assessed using the RiboGreen™ RNA Assay Kit (Thermo Fisher Scientific, Waltham, MA, USA), following the manufacturer's instructions. Briefly, 50 μL of each sample was transferred into black 96-well plates (Corning Inc., Corning, NY, USA), either in the presence (+) or absence (−) of 0.1% (w/v) Triton X-100 (Sigma-Aldrich, St Louis, MO, USA), to quantify total and unencapsulated mRNA, respectively. Samples were incubated at 37 °C for 15 minutes before the addition of RiboGreen dye. For wells containing Triton X-100, the dye was diluted 1 : 200, while a 1 : 500 dilution was used for wells without Triton. Fluorescence intensity was measured using a GloMax® Discover Microplate Reader (Promega Corporation, Madison, WI, USA), with excitation and emission wavelengths set to 480 and 520 nm, respectively. Encapsulation efficiency (%) was calculated from a standard curve prepared under both conditions, using the following equation:

$$\text{Encapsulation efficiency (EE\%)} = \frac{\text{Total mRNA} - \text{Uncapsulated mRNA}}{\text{Total mRNA}} \times 100\%$$

Cellular uptake and *in vitro* expression assays

Uptake assays were performed using HEK293 cells (ATCC, LGC Standards, Teddington, UK) and PolyA-loaded LNPs containing 1 mol% $DiIC_{18}(3)$ (Invitrogen, Thermo Fisher Scientific, Loughborough, UK). Briefly, 100 μL of HEK293 cells at 80% confluence were seeded in black 96-well plates (Corning Inc., supplied by Sigma-Aldrich, Gillingham, UK) at a density of 1.5×10^4 cells per well and incubated at 37 °C with 5% CO_2 for 48 hours. Cells were then treated with 100 μL of LNPs at concentrations ranging from 0.25 to 2 μg mL^{-1} for 24 hours. Following incubation, cells were lysed with 2% Triton X-100 (Merck Life Science, Hertfordshire, UK) in PBS for 10 minutes. Fluorescence intensity was measured using a GloMax® Discover Microplate Reader (Promega UK, Southampton, UK) to quantify LNP uptake. A linear calibration curve was established for LNP concentrations up to 500 ng mL^{-1} ($R^2 \geq 0.998$).

To evaluate mRNA expression, an *in vitro* firefly luciferase (FLuc) mRNA expression assay was conducted using HEK293 cells. As above, 100 μL of cells at 80% confluence were seeded into 96-well plates at a density of 1.5×10^4 cells per well and incubated for 48 hours at 37 °C with 5% CO_2. Cells were then treated with FLuc mRNA-loaded LNPs at concentrations ranging from 0.25 to 2 μg mL^{-1} for 24 hours. Following treatment, 100 μL of ONE-Glo™ Luciferase Assay Reagent (Promega UK, Southampton, UK) was added directly to each well. Luminescence was recorded using the GloMax® Discover Microplate Reader to assess mRNA translation efficiency.

In vivo bioluminescence imaging

Fluc mRNA-loaded LNPs were used to assess bioluminescence *in vivo* expression profile. Female BALB/c mice (aged 6–9 weeks) were housed under standard conditions, including a temperature of 22 °C, 55% humidity, and a 12-hour light/dark cycle. They had

unrestricted access to a standard diet. Each mouse received an intramuscular injection of 50 μL (100 μg mL^{-1} mRNA) into both quadriceps. Bioluminescence imaging was conducted using the IVIS Spectrum Imaging System (Revvity, Waltham, MA, USA), and data were captured and analysed using Living Image® software. Firefly luciferase expression (emission at 560 nm) was detected using medium binning and an f/stop of 2. Image acquisition time was determined automatically using the auto-exposure setting. Mice were anaesthetised using 3% isoflurane for induction and maintained at 2.5% throughout the imaging procedure. Imaging was conducted at 0.25, 6, 24, and 48 hours post-injection. The total photon flux (photons per second) was quantified for each mouse at the injection site using a defined region of interest (ROI).

Immunisation and sample collection

Groups of five female BALB/c mice (6–9 weeks old) were immunised intramuscularly on days 0 and 28 with 50 μL (containing 5 μg mRNA per dose) injected into the right quadricep of each mouse. The mRNA encoded ovalbumin (OVA) was formulated into the five different LNP compositions (Table 1). Blood samples were collected from individual mice on days 0 (before immunisation), 27 (one day before the booster dose), and 42 (two weeks after the booster dose) for serological analysis. Spleens were harvested from all animals on day 42 to enable *in vitro* T-cell assays.

Enzyme-linked immunosorbent assay (ELISA)

Blood samples collected throughout the study were analysed to assess the ability of each LNP formulation to induce serum-specific IgG isotype responses (total IgG, IgG1, and IgG2a), following the method previously described.[9] Briefly, ovalbumin (OVA) from chicken egg white (Merck Life Science UK, Hertfordshire, UK) was used to coat 96-well microtitre plates (Greiner Bio-One GmbH, Frickenhausen, Germany) at a concentration of 1 μg mL^{-1} in PBS (pH 9.0). Plates were incubated overnight at 4 °C. After incubation, plates were washed three times with wash buffer (PBS, pH 7.4, containing 0.05% Tween-20). To block non-specific binding, 150 μL of a 4% (w/v) Marvel® skimmed milk powder solution in PBS (pH 7.4) was added per well, followed by incubation at 37 °C for 1 hour. Plates were rewashed, and 100 μL of serially diluted serum samples were added to designated wells and incubated at 37 °C for 1 hour. After washing, 100 μL per well of horseradish peroxidase (HRP)-conjugated goat anti-mouse antibodies specific for total IgG (1 : 2500), IgG1 (1 : 5000), or IgG2a (1 : 5000) in PBS (pH 7.4) containing 10% (v/v) fetal calf serum (FCS) were added. The plates were incubated for an additional hour at 37 °C, followed by washing. Next, 100 μL of TMB substrate (Fisher Scientific, Loughborough, UK) was added to each well and incubated at room temperature for 20 minutes. The reaction was terminated with 10% aqueous sulfuric acid, and the absorbance was measured at 450 nm using a Microplate Manager reader (Bio-Rad Laboratories, Hercules, CA, USA). Endpoint titres were calculated and reported as mean ± Standard Error of the Mean (SEM) for each group.

Spleen cell isolation and *ex vivo* restimulation assay

Following euthanasia, spleens were aseptically removed from mice and processed to generate single-cell suspensions in incomplete RPMI-1640 medium (supplemented with 100 μg mL^{-1} penicillin–streptomycin and 200 mM L-glutamine; Thermo Fisher Scientific, Loughborough, UK). Spleens were mechanically dissociated by gently pressing them through a sterile Nitex mesh filter using the blunt end of a 2.5 mL syringe. The resulting cell suspension was transferred into labelled universal tubes and centrifuged at 300*g* for 5 minutes at 4 °C using a BioFuge Fresco centrifuge (Heraeus Instruments, Thermo Scientific, UK). The cell pellet was resuspended in 3 mL of Boyle's solution (0.007 M NH_4Cl, 0.0085 M Tris, pH 7.2) and incubated at room temperature for 5 minutes to lyse red blood cells. Cells were pelleted again under the same centrifugation conditions and washed twice with RPMI-1640 medium to ensure complete removal of residual lysis buffer. The final cell pellet was resuspended in 1 mL of complete RPMI-1640 medium (supplemented with 10% fetal calf serum; Sigma-Aldrich, Gillingham, UK), and total viable cell counts were determined by trypan blue exclusion, with viability consistently exceeding 97%. For restimulation assays, spleen cells (5×10^5 per well) were seeded into 96-well tissue culture plates (Corning Inc., supplied by Sigma-Aldrich, Gillingham, UK) and cultured under three different conditions: medium alone (unstimulated control), soluble antigen (5 μg mL^{-1} OVA in PBS, pH 7.4), or concanavalin A (10 μg mL^{-1}, positive control; Sigma-Aldrich, UK). Each well contained a final volume of 200 μL. Plates were incubated at 37 °C in a humidified atmosphere of 5% CO_2 and 95% air for 72 hours. After incubation, plates were stored at −20 °C until cytokine levels could be measured.

Cytokine quantification by ELISA

Cytokine concentrations in cell culture supernatants were quantified using enzyme-linked immunosorbent assays (ELISA) specific for mouse IFN-γ, following standard protocols. Ninety-six-well ELISA plates (Nunc MaxiSorp™, Thermo Fisher Scientific, Loughborough, UK) were coated with 50 μL per well of rat anti-mouse cytokine capture antibody (2 μg mL^{-1} in PBS, pH 9.0) specific for IFN-γ and incubated overnight at 4 °C. Plates were washed three times with wash buffer (PBS, pH 7.4, containing 0.05% Tween-20) and blocked with 150 μL of PBS containing 10% (v/v) foetal calf serum (FCS; Sigma-Aldrich, Gillingham, UK) per well for 1 hour at 37 °C. After washing, 30 μL of either cell culture supernatant or serially diluted cytokine standards (starting at 20 ng mL^{-1} in PBS with 10% FCS) were added to the appropriate wells and incubated at 37 °C for 2 hours. Following another wash step, 100 μL per well of biotin-conjugated rat anti-mouse detection antibody (1 μg mL^{-1} in PBS with 10% FCS) was added and incubated for 1 hour at 37 °C. Plates were washed three times before adding 100 μL per well of streptavidin-HRP conjugate (1 : 4000 dilution in PBS with 10% FCS), followed by a further 1-hour incubation at 37 °C. After a final wash, 100 μL of TMB substrate solution

(Fisher Scientific, Loughborough, UK) was added to each well. The reaction proceeded at room temperature in the dark for 20–60 minutes. The reaction was stopped with 10% aqueous sulfuric acid, and the absorbance was measured at 405 nm using a microplate reader (Bio-Rad Laboratories, Hercules, CA, USA). Cytokine concentrations (ng mL^{-1}) were calculated using standard curves from the known cytokine standards run on the same plate. Data are reported as mean ± Standard Error of the Mean (SEM) for each condition.

Ex vivo blood exposures

Blood was collected fresh from healthy volunteers in tubes containing the anticoagulant Li-heparin under the Liverpool PharmB ethics approval, which allows for *in vitro* assessments of immune responses to complex medicines. Within 30 minutes of being drawn, the blood was diluted 1 : 4 with complete culture media (RPMI-1640 10% v/v FBS), 400 μL of diluted blood was then seeded into 48-well plates, and 100 μL of each test compound diluted in media was added. The final concentrations of SM-102 in all 5 LNPs tested were 5, 10, and 20 μg mL^{-1}. Plates were incubated for 24 hours at 37 °C, 5% CO_2. Samples were then centrifuged at 860*g* for five minutes, and 100 μL aliquots of the supernatants were frozen at −80 °C until analysis.

Luminex panel analysis

Supernatants were thawed, and cytokine analysis was performed using the Human Magnetic Luminex Assay protocol. Samples, standards and all reagents were allowed to equilibrate to 15–30 °C. The standards provided in the kit were reconstituted with Calibrator Diluent RD6-52 using the volumes specified on the certificate of analysis and allowed to stand for 15 minutes with gentle agitation. 100 μL of each was then combined with Calibrator Diluent RD6-52 to make it up to 1 mL to create standard 1. A 3-fold dilution series in Calibrator Diluent RD6-52 was performed to develop five further standards. The wash buffer was made by adding 20 mL of wash buffer concentrate to 480 mL of distilled water. Samples were centrifuged at 860*g* for 5 minutes, and 50 μL of sample or standard was plated in its respective well; all standards and samples were read in duplicate. The human magnetic microparticle cocktail was vortexed, and 500 μL was added to 5 mL of Diluent RD2-1 to create the diluted microparticle cocktail. 50 μL of microparticle cocktail was added to every well on the 96-well plate and incubated at room temperature on a plate shaker set at 800 RPM for two hours. The plate was washed thrice with the addition and aspiration of 100 μL of wash buffer on the Bio-Plex Pro II wash station. 500 μL Biotin-antibody cocktail was added to 5 mL of Diluent RD2-1 to create the diluted biotin–antibody cocktail. 50 μL of diluted Biotin antibody cocktail was added to each well and incubated at room temperature on a plate shaker set at 800 RPM for one hour. During this incubation, the Bio-Plex 200 Luminex was calibrated, and bead regions/standard values were entered into the software. Streptavidin-PE concentrate was vortexed, and 220 μL was added to 5.35 mL of Wash buffer in a polypropylene test tube wrapped with aluminium foil to protect it from light. The plate wash was repeated, and 50 μL of diluted streptavidin-PE was added to each well and incubated at 15–30 °C on a plate shaker set at 800 RPM for 30 minutes. The plate wash was repeated, and 100 μL of wash buffer was added to each well and incubated for two minutes on a plate shaker set to 800 RPM. The plate was analysed using the Bio-Plex 200 Luminex, setting the sample volume at 50 μL, bead type as Bio-Plex MagPlex Beads, setting double discriminator gates at 8000 and 23000, reporter gain settings set to low RP1 target value for CAL2 setting, 50 counts per region and collecting median fluorescence intensity (MFI).

Ethics statement

Animal experiments and experimental procedures were carried out in line with UK Home Office regulations and the University of Strathclyde Animal Welfare and Ethical Review Board regulations under project license number PPL PP1650440. BALB/c mice were all bred and maintained in the Biological Procedures Unit at the University of Strathclyde, Glasgow and experimental design and reporting adhered to the ARRIVE guidelines. Healthy blood samples from healthy volunteers at the University of Liverpool were collected through venipuncture by trained staff, with all protocols and procedures approved by the University Research Ethics Committee (REC) approval number 11499, termed the Pharmacology Biobank (PHARM B). This ethics approval permits the collection of blood from healthy volunteers and the isolation of immune cells and blood products for profiling immune responses to complex medicines, both *in vitro* and *ex vivo*.

Statistical analysis

Results are represented as mean ± SD or ± SEM of at least $n = 3$ independent batches. One-way ANOVA tests were used to assess statistical significance, with a Kruskal–Wallis test and Dunn's multiple comparisons test (p-value of less than 0.05).

Results and discussion

Formation of LNPs

Five LNP formulations with different combinations of helper lipids and sterols were evaluated for their physicochemical properties, including particle size, polydispersity index (PDI), zeta potential, and encapsulation efficiency (EE%). The results are summarised in Table 2. All formulations produced LNPs with average diameters below 120 nm, low PDI (≤0.1) and near-neutral zeta potentials. Formulations containing either cholesterol or DOPE produced smaller LNPs (85–100 nm) than the formulation containing β-sitosterol, which had an average size of 111 ± 7.5 nm (Table 2). All five formulations exhibited high encapsulation efficiency (>95%), as expected, given that they all used the same ionisable lipid (SM-102) ratio. Gel electrophoresis verified the integrity of the mRNA (Fig. S1).

All LNPs were produced using the same microfluidic mixing process, likely contributing to the consistent physico-

Table 2 Physicochemical characteristics of LNPs prepared with different phospholipid and sterol combinations. LNPs were formulated using a consistent microfluidic mixing process and characterised for average particle diameter, polydispersity index (PDI), zeta potential, and encapsulation efficiency (EE%). Data are presented as mean ± SD of 3 independent studies

Formulation	Average diameter (nm)	PDI	Zeta potential (mV)	EE%
DSPC/Chol	90.1 ± 4.1	0.07 ± 0.04	−1.3 ± 0.5	96 ± 0.7
DOPC/Chol	89.8 ± 1.9	0.08 ± 0.09	3.6 ± 5.1	99 ± 0.1
DSPC/DOPE	97.0 ± 9.4	0.10 ± 0.02	7.4 ± 0.3	99 ± 0.1
DOPC/DOPE	85.2 ± 3.2	0.10 ± 0.02	6.5 ± 2.7	99 ± 0.1
DSPC/β-sito	111 ± 7.5	0.06 ± 0.03	−1.4 ± 5.3	99 ± 0.1

chemical properties observed across formulations, as we have previously shown that the choice of mixer is a driving factor in the phyisco-chemical characteristics of LNPs.[10] The observed similarity in size distribution, PDI, and encapsulation efficiency reflects the reproducibility and control offered by microfluidic mixing.

Importantly, the type of mixer used during nanoprecipitation exerts substantial control over the physicochemical properties of LNPs.[11–13] For example, a recent study by our group compared low-cost microfluidic mixers, including T junction and confined impingement–jet designs, with manual pipette mixing. The study demonstrated that all methods produced particles in the 95–215 nm range with high encapsulation (70–100%).[10] However, in-depth analytics revealed clear distinctions in size distribution and structural heterogeneity depending on mixer type. Notably, microfluidic mixers yielded tighter size distributions and more homogeneous internal structures, whereas pipette mixing generated broader distributions but still provided adequate performance for small-scale screening.

However, the slightly larger particle size observed in the β-sitosterol-containing formulation may be attributed to the bulkier sterol structure compared to cholesterol, potentially altering lipid packing and membrane curvature during nanoparticle formation.[14] Whilst not seen in our data (Table 1), the choice of phospholipid has been reported to play a key role in stabilising LNP structure and in dispersion characteristics. For instance, it was reported that LNPs containing DOPE exhibited higher polydispersity across all RNA cargo types tested compared with formulations containing DSPC.[15]

In vitro cellular transfection efficiency and uptake of LNP formulations

To evaluate the *in vitro* performance of the different LNP formulations, transfection efficiency and cellular uptake were measured in HEK-293 cells following treatment with mRNA-loaded LNPs across a range of concentrations (2, 1, 0.5, and 0.25 μg mL^{-1}) (Fig. 2). As shown in Fig. 2A, most formulations exhibited a dose-dependent increase in luciferase expression. However, DSPC/β-sitosterol LNPs expression profiles peaked at 1 μg mL^{-1}, potentially due to saturation of the expression processes. At all concentrations tested, DSPC/β-sitosterol LNPs produced significantly higher expression than the control DSPC/Chol LNPs ($p < 0.05$).

Cellular uptake, measured using DilC-labelled LNPs (Fig. 2B), did not mirror the trends observed for transfection efficiency. While DSPC/β-sitosterol LNPs demonstrated the highest expression, uptake levels were broadly similar across all formulations, with no significant differences observed. Increasing the LNP dose from 0.25 to 2 μg mL^{-1} led to a consistent decrease in cellular fluorescence across all formulations (Table S1), which may reflect a combination of fluorescence quenching at high DiI concentrations and cellular regulation of uptake (*e.g.* surface saturation or reduced endocytosis).

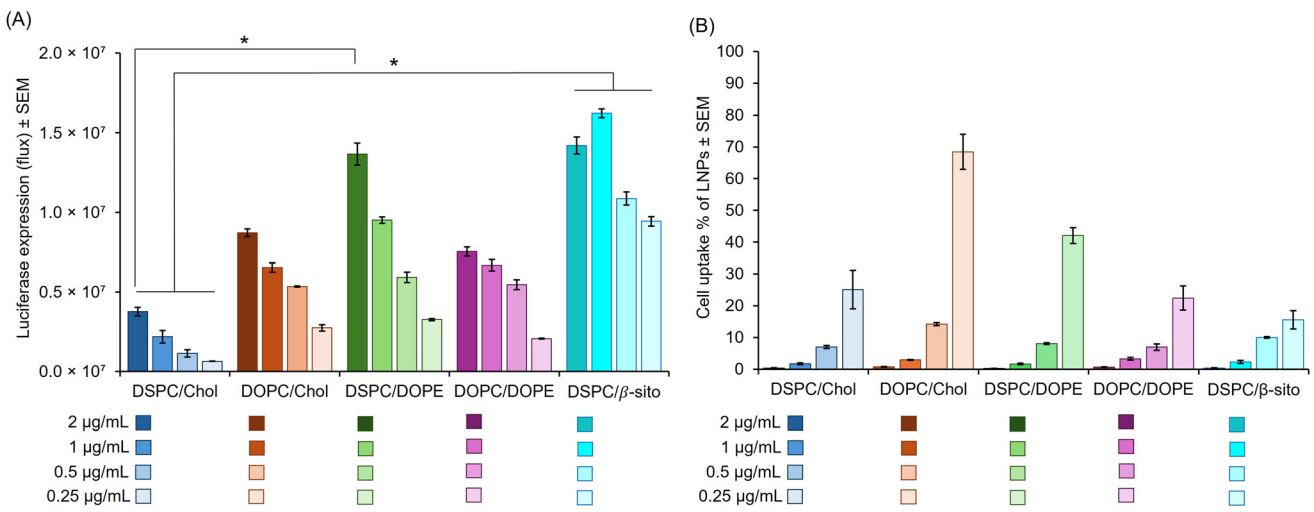

Fig. 2 *In vitro* characterisation of mRNA-LNP formulations: transfection efficiency and uptake. (A) Firefly luciferase (Fluc) expression was measured in HEK293 cells 48 h after transfection with mRNA-LNP formulations containing different combinations of phospholipids (DSPC, DOPC, DOPE) and sterols (cholesterol, β-sitosterol) (see Table 1). (B) Cellular uptake of DilC-labelled LNP formulations. Data represent mean ± SEM from three independent experiments. Statistical analysis was performed using the Kruskal–Wallis test, followed by Dunn's *post hoc* test for multiple comparisons.

Cytotoxicity was ruled out as a contributing factor, as viability remained unchanged across all conditions (Fig. S2).

These findings align with literature showing that sterol identity can strongly influence LNP performance *in vitro*. β-Sitosterol differs from cholesterol by an additional C24 ethyl group, introducing steric effects that disrupt lipid packing and alter membrane fluidity, thereby facilitating endosomal escape. Indeed, Patel *et al.*[7] reported superior gene expression and delivery with β-sitosterol-based LNPs without compromising encapsulation efficiency or stability, and Medjmedj *et al.*[14] similarly found that replacing cholesterol with β-sitosterol enhanced mRNA expression in immortalised cell lines. Our findings are consistent with this: DSPC/β-sitosterol LNPs outperformed DSPC/Chol despite similar uptake, suggesting enhanced intracellular trafficking and release.

At the highest concentration tested (2 μg mL^{-1}), substituting cholesterol with DOPE in the LNP formulation also resulted in a significant increase in luciferase expression compared to the control DSPC/Chol LNP formulation (Fig. 2A). Other formulation changes had no significant impact on expression relative to the control DSPC/Chol LNPs. This improvement can be attributed to DOPE's cone-shaped geometry that enhances membrane fusion and endosomal escape.[2,4] DOPE adopts a cone-shaped geometry due to its unsaturated acyl chains, which favours the formation of non-lamellar phases under acidic conditions in the endosome. This biophysical behaviour supports destabilisation of the endosomal membrane, facilitating escape of the mRNA into the cytosol.[4]

Consistent with this, Barbieri *et al.*[16] demonstrated an increase in the *in vitro* potency of DOPC- and DOPE-containing formulations compared to DSPC formulations in MC3 and C12-200 LNPs in some cell lines. Molecular dynamics simulations[17] further illustrate how such differences in potency may arise from the distinct molecular interactions of helper lipids with ionisable lipids such as DLin-MC3-DMA. The results showed that DOPE, owing to its smaller headgroup, interacts more strongly with the tails and carbonyl oxygens of DLin-MC3-DMA than DOPC, positioning the ionisable lipid closer to the membrane surface. These interactions altered membrane organisation, with DOPE-containing bilayers exhibiting reduced water penetration and slower lipid diffusion compared to DOPC bilayers. Such structural and dynamic differences provide a molecular basis for how helper lipid chemistry can modulate LNP architecture and behaviour.

In vivo expression kinetics of LNP formulations following intramuscular injection

To evaluate the *in vivo* performance of the different LNP formulations, BALB/c mice were injected intramuscularly with 5 μg of Fluc mRNA-LNPs, and luciferase activity was monitored over 48 hours using IVIS imaging (Fig. 3). Peak expression at the injection site was observed at 6 hours for all formulations, followed by a decline at 24 and 48 hours (Fig. 3A). DSPC/Chol LNPs produced the highest signal at the injection site, followed by DSPC/β-sitosterol and DOPC/Chol. In contrast, DOPE-containing formulations (DSPC/DOPE and DOPC/DOPE) yielded substantially lower expression levels.

To better compare overall expression, the area under the curve (AUC) for the 0.25–48 h time period was calculated for each mouse (Fig. 3B). DSPC/Chol LNPs exhibited the highest AUC values, followed by DSPC/β-sitosterol and DOPC/Chol formulations, which showed comparable expression (Fig. 3B). However, all LNP formulations had significantly reduced AUC values compared to DSPC/Chol LNPs ($p < 0.05$, Dunn's test with Holm correction), suggesting lower overall protein output *in vivo*, despite their high *in vitro* potency.

Liver expression was also measured at the 6-hour timepoint (Fig. 3C). While the luciferase signal was high and not significantly different in the liver for DSPC/Chol, DOPC/Chol, and DSPC/β-sitosterol LNPs, the DOPE-containing LNPs showed minimal hepatic expression. Among the tested formulations, DOPC/Chol and DSPC/β-sitosterol LNPs exhibited liver expression comparable to that of DSPC/Chol LNPs. Representative IVIS images illustrate these patterns (Fig. 3D), with clear differences in signal intensity and anatomical localisation.

In contrast to the highlighted superior performance for β-sitosterol-containing LNPs *in vitro* (Fig. 2), the *in vivo* results reveal a more nuanced picture. DSPC/Chol LNPs yielded the highest overall luciferase expression at the injection site, but DSPC/β-sitosterol LNPs achieved comparable levels of expression at 6 h and showed similar hepatic expression to DSPC/Chol LNPs. This indicates that β-sitosterol can support *in vivo* mRNA delivery to a similar extent as cholesterol in certain formulation contexts, though without the enhanced expression seen *in vitro* (Fig. 2).

By comparison, DOPE-containing LNPs displayed consistently reduced expression at both the injection site and in the liver. This may reflect differences in biodistribution and/or colloidal stability *in vivo*. Furthermore, the reduced liver expression observed with DOPE-containing LNPs may simply be a consequence of the reduced overall potency of these formulations. As noted, DOPE possesses unsaturated (oleoyl) acyl chains and a relatively small headgroup, which gives it a cone-shaped geometry that can promote ensodosmal escape *in vitro*.[4] However, *in vivo*, the same fusogenic properties can destabilise the LNP structure, making them more prone to lipid desorption, aggregation, or premature clearance. As a result, DOPE-LNPs underperformed relative to DSPC- or DOPC-containing formulations despite their higher performance *in vitro* (Fig. 2). Indeed, the poor correlation between *in vitro* and *in vivo* performance of helper lipids has been shown by Barbieri *et al.*,[16] who demonstrated that although DOPE-containing LNPs achieved the highest *in vitro* transfection levels, their *in vivo* expression in murine muscle and skin explants was inferior to DSPC-containing counterparts, which offered enhanced formulation stability and expression durability. This discrepancy reinforces the growing recognition that *in vitro* potency does not reliably predict *in vivo* expression.[16,18]

In vivo immunogenicity of LNP formulations following prime-boost vaccination

To assess the immunogenicity of the five mRNA-LNP formulations, BALB/c mice were immunised intramuscularly with

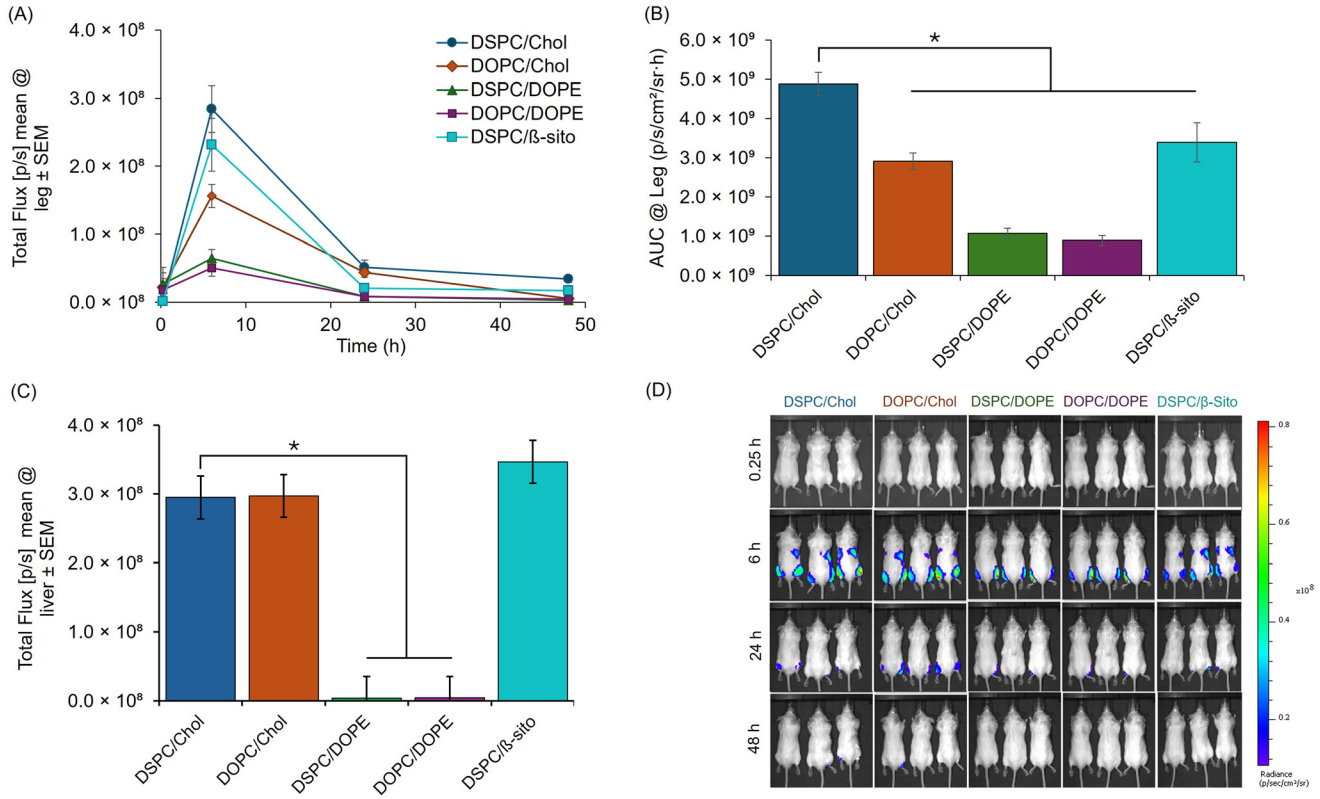

Fig. 3 *In vivo* luciferase expression following intramuscular injection of mRNA-LNP formulations in BALB/c mice. Mice were injected intramuscularly with 5 μg of Fluc mRNA formulated in LNPs containing different combinations of phospholipids (DSPC, DOPC, DOPE) and sterols (cholesterol or β-sitosterol) (Table 1). (A) Time-course of luciferase expression at the injection site over 48 hours. (B) Area under the curve (AUC) of total luciferase expression at the injection site. (C) Luciferase expression in the liver at 6 hours post-injection. (D) Representative IVIS images of mice at each time point (0.25, 6, 24, and 48 h). Colour scale indicates radiance intensity (p s^{-1} cm^{-2} sr^{-1}). Statistical analysis for AUC and liver expression was performed using the Kruskal–Wallis test followed by pairwise Mann–Whitney *U* tests with Holm correction for multiple comparisons. Significant differences relative to DSPC/Chol are annotated where $p < 0.05$. Data are expressed as mean ± SEM (6 mice per formulation, split over 2 independent studies).

5 μg of OVA-encoding mRNA formulated in each LNP formulation (Table 1). Mice received a prime dose on day 0 and a booster on day 28. Blood samples were collected at day 27 post-prime and day 42 (two weeks after boosting). The study was terminated on day 42, when antibody titres were measured by ELISA, and splenocytes were harvested for cytokine analysis following OVA peptide stimulation (Fig. 4).

On day 27, one day before the booster dose, all LNP formulations elicited low and comparable antibody responses. However, by day 42 (two weeks post-booster), antibody responses against the encoded antigen were observed with all formulations (Fig. 4B–D). Among them, the DSPC/DOPE LNPs induced significantly higher total IgG titres ($P < 0.05$) than the benchmark DSPC/Chol LNPs, followed by DOPC/DOPE and DOPC/Chol LNPs. DSPC/Chol and DSPC/β-sitosterol LNPs generated comparable total IgG levels, albeit lower than the DOPE- and DOPC-containing formulations (Fig. 4B). IgG1 responses showed a similar trend (Fig. 4C), whereas for IgG2a (Fig. 4D), DOPC/DOPE LNPs generated the highest titres, followed by DSPC/Chol, DOPC/Chol, and DSPC/β-sitosterol LNPs, which produced comparable intermediate levels. DSPC/DOPE LNPs generated the lowest IgG2a responses.

IFN-γ production by antigen-stimulated splenocytes (Fig. 4E) broadly mirrored IgG2a responses, with DSPC/DOPE promoting lower levels compared to the other LNP formulations. BALB/c mice are generally Th2-prone; however, under Th1-inducing conditions, IFN-γ promotes class switching to IgG2a. In this strain, elevated IFN-γ is therefore closely linked with enhanced IgG2a production, marking a coordinated shift towards cellular and humoral Th1 immunity.[19]

These findings demonstrate that LNP composition influences not only *in vivo* protein expression but also the magnitude and quality of the resulting adaptive immune response in mice. Importantly, there was no direct correlation between *in vivo* luciferase expression and immunogenicity. For instance, DSPC/Chol LNPs produced the highest protein expression (Fig. 3), yet elicited relatively modest antibody IgG and IgG1 responses compared to DSPC/DOPE and DOPC/DOPE LNPs (Fig. 4B and C). Furthermore, while all five formulations could induce antigen-specific IgG following a prime-boost immunisation, distinctions in total IgG, subclass profiles, and IFN-γ secretion highlight formulation-dependent immune modulation.

Another important consideration is that luciferase and ovalbumin may exhibit different *in vivo* expression kinetics, which

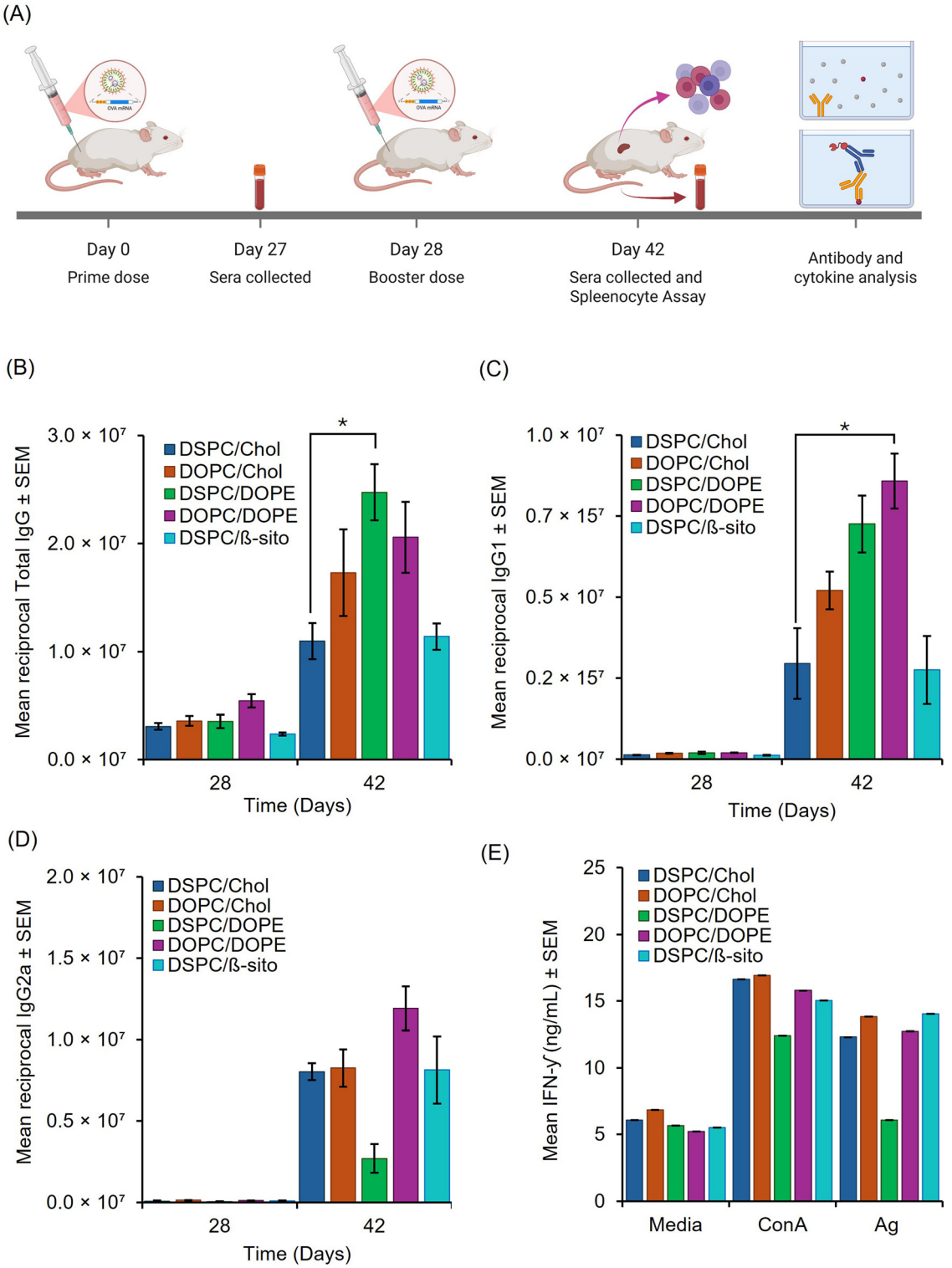

Fig. 4 Evaluation of vaccine-induced immune responses following intramuscular administration of mRNA-LNPs in mice. BALB/c mice were immunised intramuscularly with 5 μg of OVA-encoding mRNA formulated in different LNP compositions on day 0 (prime) and day 28 (boost). (A) Schematic of the vaccination and sample collection protocol. (B) Total anti-OVA IgG titres measured by ELISA at days 27 (pre-boost) and 42 (two weeks post-boost). (C) IgG1 and (D) IgG2a subclass titres measured by ELISA at the same timepoints. (E) IFN-γ secretion by splenocytes harvested at day 42 and restimulated *ex vivo* with OVA peptide, quantified by sandwich ELISA. Data are presented as mean ± SEM (n = 5 mice per group). Statistical analysis was performed using the Kruskal–Wallis test followed by Dunn's *post hoc* test for multiple comparisons. Significant differences relative to DSPC/Chol are annotated where $p < 0.05$.

could also contribute to the lack of correlation between Fig. 3 and 4. Luciferase is a small reporter protein that is rapidly expressed and degraded, and its activity is typically detectable shortly after delivery but declines quickly.[20] In contrast, ovalbumin is a larger, more stable antigen with potentially slower expression onset but prolonged availability for antigen presentation. As a result, the timing, duration, and localisation of expression may differ substantially between these two proteins. This could contribute to the disconnect between expression (Fig. 3) and immunogenicity (Fig. 4). Indeed, we have previously shown that luciferase expression at the injection site does not necessarily correlate with immune responses to the encoded antigen (OVA).[18]

This disconnect between expression and immunogenicity is further supported by Zhang *et al.*,[21] who compared three LNP formulations for mRNA delivery using firefly luciferase as a model antigen. Although SM-102 and ALC-0315 LNPs demonstrated high levels of luciferase expression following intramuscular injection, only these two formulations elicited substantial luciferase-specific antibody responses, whereas KC2-based

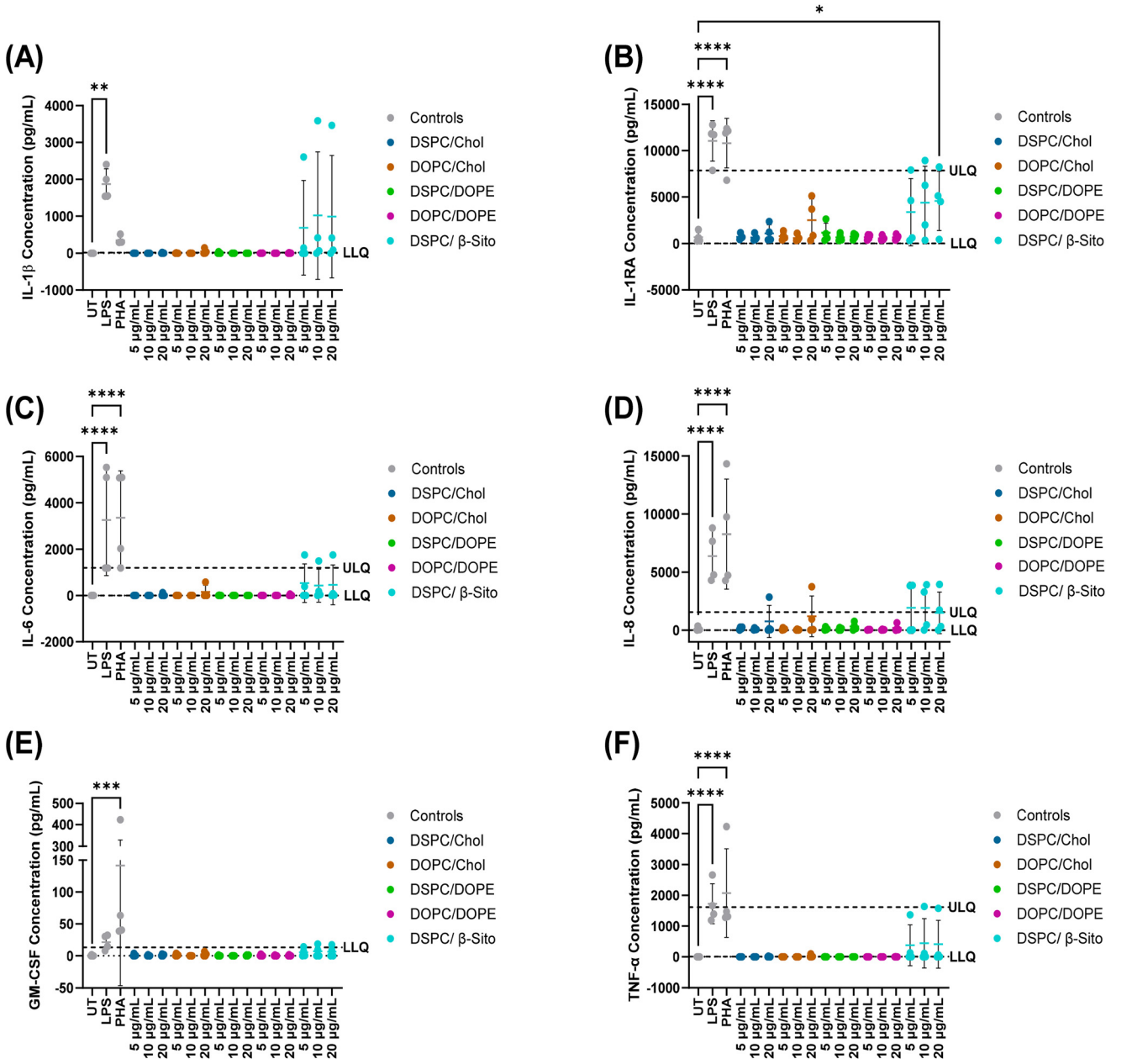

Fig. 5 LNPs exposed to healthy donor whole blood for 24 hours and supernatant cytokines measured *via* Luminex assay. (A) IL-1β, (B) IL-1RA, (C) IL-6, (D) IL-8, (E) GM-CSF, (F) TNF-α. Upper limit of Quantification and Lower limit of quantification are denoted by the dashed line and ULQ and LLQ, respectively. n = 3 donors, with each donor average being an average of 2 technical replicates. ANOVA statistical analysis carried out between the untreated and all other conditions, $p < 0.0001$ = ****, $p < 0.001$ = ***, $p < 0.01$ = ** and $p < 0.05$ = *.

LNPs, which promoted lower but still notable expression, produced negligible antibody titres. These findings reinforce that protein expression alone does not determine immunogenicity and that the LNP formulation itself can shape both innate and adaptive immune responses. Indeed, recent studies have shown that ionisable lipid chemistry directly influences immunogenicity *via* engagement of immune receptors such as TLR4 and CD1d.[22] By contrast, helper lipids such as DOPE and DOPC are not direct pattern recognition receptor agonists but could modulate immunogenicity indirectly through effects on membrane structure, trafficking, and biodistribution.

Thus, the immunostimulatory nature of the components may contribute to enhanced local inflammation or antigen-presenting cell activation, which could promote stronger adaptive responses even with lower protein output. Including DOPE as a helper lipid in both DSPC/DOPE and DOPC/DOPE LNPs enhanced humoral responses, inducing higher total IgG and IgG1 titres. However, DSPC/DOPE showed weaker IgG2a and IFN-γ responses than other formulations, suggesting a Th2-skewed immune profile. DOPC/DOPE LNPs, on the other hand, induced strong IgG1 and IgG2a titres along with high IFN-γ levels, suggesting a more balanced Th1/Th2 response profile.

DSPC/β-sitosterol LNPs produced similar immune response profiles to DSPC/Chol LNPs. Thus, despite the ability of β-sitosterol to enhance endosomal escape and improve mRNA delivery and protein expression[7] its incorporation conferred limited immunological advantage in this vaccine context.

Cytokine responses to LNPs, *ex vivo*, in human blood

These immunogenicity studies in mice demonstrate that lipid composition plays a critical role not only in antigen expression but also in shaping the balance between Th1- and Th2-type responses. These findings raise important questions about the mechanisms underlying these immune polarisation effects, particularly the role of early innate immune activation in modulating downstream adaptive responses. To begin addressing this, we next evaluated how these same LNP formulations affect innate cytokine responses *ex vivo* in human whole blood (Fig. 5).

Therefore, to study human proinflammatory cytokine responses to these LNPs, healthy donor volunteer blood was used, and six cytokines were measured *via* Luminex assay: IL-1β, IL-1RA, IL-6, IL-8, TNF-α and GM-CSF. DSPC/β-sitosterol LNPs at 20 μg mL^{-1} SM-102 concentration caused significantly higher production of IL-1RA when compared to the untreated, 562% higher. DSPC/β-sitosterol at all three concentrations tested (5–20 μg mL^{-1}) also led to notably higher IL-1β (percentages uncalculatable), IL-1RA (387%, 534%), IL-6 (54 555%, 43 527%, 46 993%), IL-8 (1434%, 1428%, 1094%), GM-CSF (1089%, 1383%, 1295%) and TNF-α (22 738%, 26 588%, 24 861%) secretion with all three concentrations tested (5–20 μg mL^{-1}). DSPC/Chol and DOPC/Chol at 20 μg mL^{-1} also caused notably higher IL-1RA (59%, 261%), IL-6 (3292%, 15 584%), IL-8 (509%, 852%) and TNF-α (298%, 1649%). The Luminex analysis of healthy volunteer human blood exposed to the different LNPs showed that the β-sitosterol containing LNPs and the highest concentration (20 μg mL^{-1}) of DSPC/Chol and DOPC/Chol LNPs caused a higher pro-inflammatory cytokine response when compared to the untreated. These human blood results also supported the finding that β-sitosterol containing LNPs lead to a higher Th1 stimulation, exhibited by the notably higher levels of TNF-α, GM-CSF and IL-8 at all concentrations tested.[23] β-Sitosterol containing LNPs also caused a significantly higher production of IL-1RA and notably higher IL-1β secretion at the highest concentration tested. IL-1β is a proinflammatory cytokine that is produced following inflammasome activation and has been shown to be secreted by SM-102 LNPs previously.[24] IL-1RA plays a role in the feedback mechanisms following IL-1 secretion and exerts an anti-inflammatory effect by blocking IL-1 receptors to prevent over-activation of the immune system. IL-1RA is therefore likely to be higher if IL-1β has also been secreted.[25] IL-6 also has notable secretion in the β-sitosterol treated samples; IL-6 is known to promote Th2/Th17, dependent on the presence of other cytokines and inhibit Th2 differentiation. However, it also has pro- and anti-inflammatory properties[26] and to clarify the kinetic profiles of cytokine release, multiple time points are warranted in subsequent analysis.

The *ex vivo* cytokine profiling in human whole blood highlights that β-sitosterol-containing LNPs are potent inducers of proinflammatory cytokines, including IL-1β, TNF-α, and GM-CSF cytokines known to drive Th1 polarisation. The strong induction of IL-1β and IL-1RA also suggests inflammasome activation, which may contribute to the observed immunostimulatory effects (Fig. 5).

Conclusions

This study investigates the impact of structural phospholipids and sterol analogues on the physicochemical properties, delivery efficiency, and immunological profile of mRNA-loaded LNPs. Our findings demonstrate that β-sitosterol is a viable alternative to cholesterol, achieving comparable *in vivo* expression and eliciting immune responses similar to cholesterol-based formulations. DOPE, while effective for *in vitro* transfection, resulted in poor *in vivo* expression but drove strong antibody responses, highlighting a disconnect between antigen expression and immunogenicity. These divergent outcomes highlight the complexity of lipid–lipid interactions within LNPs and caution against overreliance on *in vitro* data when predicting *in vivo* efficacy. The inclusion of *ex vivo* human blood profiling strengthens translational insight, revealing that LNP-induced cytokine signatures can predict Th1-biased responses observed *in vivo*. Altogether, our data highlight the critical, context-dependent roles of phospholipid and sterol components in shaping both delivery and immune outcomes.

Author contributions

Conceptualisation was carried out by M. H., A. M., D. B., A. H., N. L., D. M., and Y. P. Methodology was designed by M. H., A.

M., D. B., A. H., N. L., D. M., and Y. P. validation and formal analysis were performed by M. H., D. B., A. H., N. L. and Y. P. Investigation was conducted by M. H., A. M., D. B., A. H., N. L., D. M., and Y. P. Data curation was overseen by M. H., D. B., A. H., N. L., D. M., and Y. P. Writing of original draft preparation was undertaken by M. H., D. B., A. H., N. L., D. M., and Y. P. Visualisation was handled by M. H., D. B., A. H., N. L. and Y. P. All authors have read and agreed to the published version of the manuscript.

Conflicts of interest

The authors declare no conflicts of interest.

Data availability

Data for this article are available at: https://doi.org/10.15129/7ab9cd94-c69f-4cf4-bb91-2d7ad7e0c5c1.

Supplementary information is available. See DOI: https://doi.org/10.1039/d5pm00150a.

Acknowledgements

This work is part of the Intracellular Drug Delivery Centre, funded by Innovate UK (project number: 10058505).

Institutional Review Board Statement: all animal procedures were performed in accordance with the Guidelines for Care and Use of Laboratory Animals of the UK Home Office Animals Scientific Procedures Act of 1986, in accordance with an internal ethics board and UK government-approved project licence (project licence PP1650440; granted: 29 May 2020).

All experiments were performed in accordance with the Guidelines of the Central University Research Ethics Committee D, and Experiments were approved by the ethics committee at the University of Liverpool. Informed consent was obtained from all human participants in this study. This is collected by providing all information to the volunteers. Volunteers are asked whether they wish to be informed about incidental findings. Only a minimal set of personal data in pseudonymised format is stored on a secure server, with only authorised users able to access (to be able to contact the volunteer in case of incidental findings, if that has been agreed)-copies of Informed Consent/Assent Forms and Information Sheets in language and terms understandable to the participants. Participants have the right to: know that participation is voluntary; ask questions and receive understandable answers before deciding; see the degree of risk and burden involved in participation; know who will benefit from participation; understand the procedures that will be implemented in the case of incidental findings; to know how their biological samples and data will be collected, protected during the project and either destroyed or reused at the end of the research; withdraw themselves, their samples and data from the project at any time; know of any potential commercial exploitation of the research. Immune cell subsets are purified freshly (for every experiment) from volunteered human blood samples. Healthy volunteer whole blood is collected from healthy volunteers at the UoL site. UOL operates a facility (PharmB, ref# 11499, PI – Liptrott), approved by the Research Ethics Committee, that oversees the collection, handling and recording of human materials. All samples are logged with our designated individual for the Human Tissue Authority (HTA), and records are maintained to ensure that appropriate storage and disposal procedures are carried out. All SOPs for this are located within the Pharmacology department at UOL in Liverpool.

References

1 X. Hou, T. Zaks, R. Langer and Y. Dong, *Nat. Rev. Mater.*, 2021, **6**, 1078–1094.
2 C. Hald Albertsen, J. A. Kulkarni, D. Witzigmann, M. Lind, K. Petersson and J. B. Simonsen, *Adv. Drug Delivery Rev.*, 2022, **188**, 114416.
3 B. L. Mui, Y. K. Tam, M. Jayaraman, S. M. Ansell, X. Du, Y. Y. C. Tam, P. J. C. Lin, S. Chen, J. K. Narayanannair, K. G. Rajeev, M. Manoharan, A. Akinc, M. A. Maier, P. Cullis, T. D. Madden and M. J. Hope, *Mol. Ther.–Nucleic Acids*, 2013, **2**, e139.
4 P. R. Cullis and M. J. Hope, *Biochim. Biophys. Acta, Biomembr.*, 1980, **597**, 533–542.
5 R. Koynova and B. Tenchov, *Top. Curr. Chem.*, 2010, **296**, 51–93.
6 J. A. Kulkarni, D. Witzigmann, J. Leung, R. van der Meel, J. Zaifman, M. M. Darjuan, H. M. Grisch-Chan, B. Thöny, Y. Y. C. Tam and P. R. Cullis, *Nanoscale*, 2019, **11**, 9023–9031.
7 S. Patel, N. Ashwanikumar, E. Robinson, Y. Xia, C. Mihai, J. P. Griffith, S. Hou, A. A. Esposito, T. Ketova, K. Welsher, J. L. Joyal, Ö. Almarsson and G. Sahay, *Nat. Commun.*, 2020, **11**, 983.
8 S. Chatterjee, E. Kon, P. Sharma and D. Peer, *Proc. Natl. Acad. Sci. U. S. A.*, 2024, **121**, e2307800120.
9 M. Hussain, B. Binici, L. O'Connor and Y. Perrie, *J. Pharm. Pharmacol.*, 2024, **76**, 1572–1583.
10 J. Forrester, C. G. Davidson, M. Blair, L. Donlon, D. M. McLoughlin, C. R. Obiora, H. Stockdale, B. Thomas, M. Nutman, S. Brockbank, Z. Rattray and Y. Perrie, *Pharmaceutics*, 2025, **17**, 566.
11 S. J. Shepherd, X. Han, A. J. Mukalel, R. El-Mayta, A. S. Thatte, J. Wu, M. S. Padilla, M. G. Alameh, N. Srikumar, D. Lee, D. Weissman, D. Issadore and M. J. Mitchell, *Proc. Natl. Acad. Sci. U. S. A.*, 2023, **120**, e2303567120.
12 N. M. Belliveau, J. Huft, P. J. Lin, S. Chen, A. K. Leung, T. J. Leaver, A. W. Wild, J. B. Lee, R. J. Taylor, Y. K. Tam, C. L. Hansen and P. R. Cullis, *Mol. Ther.–Nucleic Acids*, 2012, **1**, e37.
13 A. Vogelaar, S. Marcotte, J. Cheng, B. Oluoch and J. Zaro, *Pharmaceutics*, 2023, **15**, 1053.

14 A. Medjmedj, A. Ngalle-Loth, R. Clemençon, J. Hamacek, C. Pichon and F. Perche, *Nanomaterials*, 2022, **12**, 2446.
15 G. B. Schober, S. Story and D. P. Arya, *Sci. Rep.*, 2024, **14**, 2403.
16 B. D. Barbieri, D. J. Peeler, K. Samnuan, S. Day, K. Hu, H. J. Sallah, J. S. Tregoning, P. F. McKay and R. J. Shattock, *J. Controlled Release*, 2024, **374**, 280–292.
17 I. Ermilova and J. Swenson, *Phys. Chem. Chem. Phys.*, 2020, **22**, 28256–28268.
18 S. Lindsay, M. Hussain, B. Binici and Y. Perrie, *Vaccines*, 2025, **13**, 339.
19 C. M. Snapper and W. E. Paul, *Science*, 1987, **236**, 944–947.
20 N. Pardi, S. Tuyishime, H. Muramatsu, K. Kariko, B. L. Mui, Y. K. Tam, T. D. Madden, M. J. Hope and D. Weissman, *J. Controlled Release*, 2015, **217**, 345–351.
21 W. Zhang, A. Pfeifle, C. Lansdell, G. Frahm, J. Cecillon, L. Tamming, C. Gravel, J. Gao, S. N. Thulasi Raman, L. Wang, S. Sauve, M. Rosu-Myles, X. Li and M. J. W. Johnston, *Vaccines*, 2023, **11**, 1580.
22 N. Chaudhary, L. N. Kasiewicz, A. N. Newby, M. L. Arral, S. S. Yerneni, J. R. Melamed, S. T. LoPresti, K. C. Fein, D. M. Strelkova Petersen, S. Kumar, R. Purwar and K. A. Whitehead, *Nat. Biomed. Eng.*, 2024, **8**, 1483–1498.
23 N. Mukaida, A. Harada and K. Matsushima, *Cytokine Growth Factor Rev.*, 1998, **9**, 9–23.
24 S. Tahtinen, A.-J. Tong, P. Himmels, J. Oh, A. Paler-Martinez, L. Kim, S. Wichner, Y. Oei, M. J. McCarron, E. C. Freund, Z. A. Amir, C. C. de la Cruz, B. Haley, C. Blanchette, J. M. Schartner, W. Ye, M. Yadav, U. Sahin, L. Delamarre and I. Mellman, *Nat. Immunol.*, 2022, **23**, 532–542.
25 W. P. Arend, M. Malyak, C. J. Guthridge and C. Gabay, *Annu. Rev. Immunol.*, 1998, **16**, 27–55.
26 S. Diehl and M. Rincón, *Mol. Immunol.*, 2002, **39**, 531–536.